metals

MDPI

Article

Electrostatic Separation of Copper and Glass Particles in Pretreated Automobile Shredder Residue

Beom-Uk Kim and Chul-Hyun Park *

Department of Energy & Resources Engineering, Chosun University, Gwangju 61452, Korea; rlaqjadnr104@naver.com

* Correspondence: chpark@chosun.ac.kr; Tel.: +82-062-230-7238

Received: 27 September 2018; Accepted: 25 October 2018; Published: 27 October 2018

Abstract: There is increasing demand for an efficient technique for separating automobile shredder residue (ASR) obtained from end-of-life vehicles (ELVs). A particular challenge is the physical separation of conductive materials from glass. In this study, the performance of pretreatment and induction electrostatic separation process was evaluated. The results show that a sieving/washing (combination of sieving and washing) pretreatment was the most effective for removing conductive material compared to electrostatic separation alone. The optimum separation efficiency of copper products was achieved with an applied voltage of 20 kV, a relative humidity of less than 35%, and a splitter position of 8 cm. Although the separation efficiency was slightly reduced when some small glass particles remained attached to the conductive materials, the separation efficiency of copper from the pretreated ASR dramatically increased to 83.1% grade and 90.4% recovery, compared to that of raw ASR (34.3% grade and 58.6% recovery). Based on these results, it was demonstrated that the proposed sieving/washing pretreatment was proficient at removing conductive materials from glass; thus, it has the potential to significantly improve the efficiency of electrostatic separation for ASR.

Keywords: ASR; pretreatments; particle trajectory; electrostatic separation

1. Introduction

End-of-life vehicles (ELVs) generally consist of 70–75% ferrous metal, 5% non-ferrous metal, and 20–25% Automobile shredder residue (ASR) is the waste produced when ELVs are shredded [1]. At present, most ASR is landfilled; however, recent legislation, such as European Directive 2000/53/EC and the resource circulation law that has been in place in Korea since 2015, requires more than 95% of the ASR produced from ELVs to be recycled [2,3].

Until now, research into mechanical/physical separation techniques for recycling ASR has primarily focused on the recovery of valuable materials using a variety of separation processes, such as electrostatic separation, eddy current separation, magnetic separation, sieving/heavy medium separation, etc. [1,4,5]. These techniques are particularly attractive as they are widely used to improve recycling efficiency in many applications.

Researchers Santini et al. reported that dense medium separation was superior to sieving by size when separating plastics from ASR prior to pyrolysis for increasing the yield of oil and gas. When pyrolysis was combined with a dense medium process, a conversion rate of over 90% (e.g., polyolefin) was achieved, which was much higher than that for raw ASR [6]. Kuwayama et al. recovered a low-density group of a 50% yield from ASR using a jig (gravity separation) with a liquid specific gravity of 1.2. The resulting group contained less than 10% ash and 2% chloride content [7]. Moreover, Alunno et al. found that sizing and magnetic separation processes were effective in removing metals from ASR and the separated inorganic materials could be utilized in the

manufacture of lightweight aggregate. When this aggregate was used to make concrete, the specific weight and compressive strength of the concrete increased by up to approximately 2000 kg/m^3 and 30 MPa, respectively, over conventional concrete [8]. Moreover, Fabrizi et al. studied a combination process using heavy medium separation, a trommel, and eddy current separation to separate cable scraps with a 75.9% recovery and 87.7% grade from ASR [9]. In particular, the addition of a nail roll was found to be a cost-effective method to separate the cable pieces and wires in the ASR. Lee et al. reported on various physical/mechanical separation techniques, such as a float-sink tank, cyclonic air separator, and electrostatic separation for recycling polymers from ASR, and specifically suggested electrostatic separation as a new and more efficient method for recycling [10].

Electrostatic phenomena have been utilized in numerous technical applications, including electro-photography, electrostatic copy and printing techniques, electrostatic filtration, precipitation, and coloring, and electrostatic separation has been used for processing valuable minerals, such as coal and fly ash, and for recycling various types of electric and electronic waste, such as printed circuit boards, cables, and plastics [11–13]. Dascalescu et al. studied electrostatic separation and conducted a trajectory simulation to evaluate the separator type, the shape of the electrode, electric field strength, and particle sizes. They also evaluated the trajectory of the copper wires contained in electric cable waste using various high-voltage electrodes and statistical software [12,14–18]. Xu et al. simulated the trajectory of a particle as a function of the shape, air drag, and various charging situations, and investigated the separation efficiency of conductors in roll-type corona electrostatic separation [19–22].

In previous works, analyses of ASR particles trajectory, a stereoscopic microscope, scanning electron microscopy, and energy dispersive X-ray spectroscopy were conducted and it was found that the electrostatic separation efficiency of the ASR deteriorated when the copper was combined with glass particles to which heterogeneous conductive materials, such as organics and metals, had adhered during the shredding process [23].

With this in mind, the focus of the current study was to develop a method of eliminating conductive materials through various pretreatments that consisted of sieving, washing, pyrolysis, oxidation, and sieving/washing. As part of the investigation, the performance of induction electrostatic separation was evaluated and various trajectory analyses of ASR after pretreatment were conducted while considering the effects of several variables, including the applied voltage, relative humidity, splitter position, and particle size.

2. Materials and Experimental

2.1. Materials

The ASR sample material used in this research consisted of non-magnetic products obtained via a series of mineral processing operations, viz., comminution, air separation, and magnetic separation, from Kyunghan Inc. in Pohang, Korea. The profile of the ASR material is listed in Table 1 and microscopic photographs of the various materials in the ASR are shown in Figure 1. The composition of the ASR sample, given in Table 1, was analyzed by handpicking. The sample comprised 10% conductors (copper, aluminum) and 90% non-conductors (glass, plastics and etc.). The conductors were approximately 9% copper and 1% aluminum, while the non-conductors were 85% glass and 5% other materials. The shapes of the copper and glass particles resembled cylinders and spheres, respectively.

Table 1. Composition of the automobile shredder residue (ASR) sample.

Materials	Copper	Aluminum	Glass	Other Materials	Total
Weight (g)	5.39	0.74	50.76	3.26	60.15
wt%	8.96	1.23	84.39	5.42	100

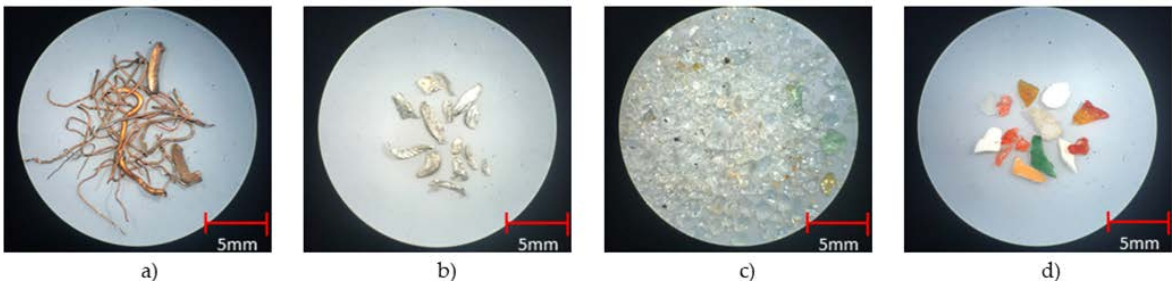

Figure 1. Microscopic photographs of various materials from automobile shredder residue (ASR). (**a**) copper, (**b**) aluminum, (**c**) glass, and (**d**) other materials.

2.2. Experiments

A flowchart of the ASR recycling process in a local plant that includes shredding and classification steps is shown in Figure 2, where it can be seen that the shredded ASR sample is separated by pneumatic separation into low- and high-gravity products. The high-gravity product is then further separated via magnetic separation into magnetic and non-magnetic products. Finally, the non-magnetic product is separated via induction electrostatic separation into conductor and non-conductor elements. It should be noted that the separation efficiency of the electrostatic separation process deteriorated, due to the presence of heterogeneous conductive materials, such as organics and metals, which became attached to the glass particles during shredding. Reversing this degradation is the focus of the current work.

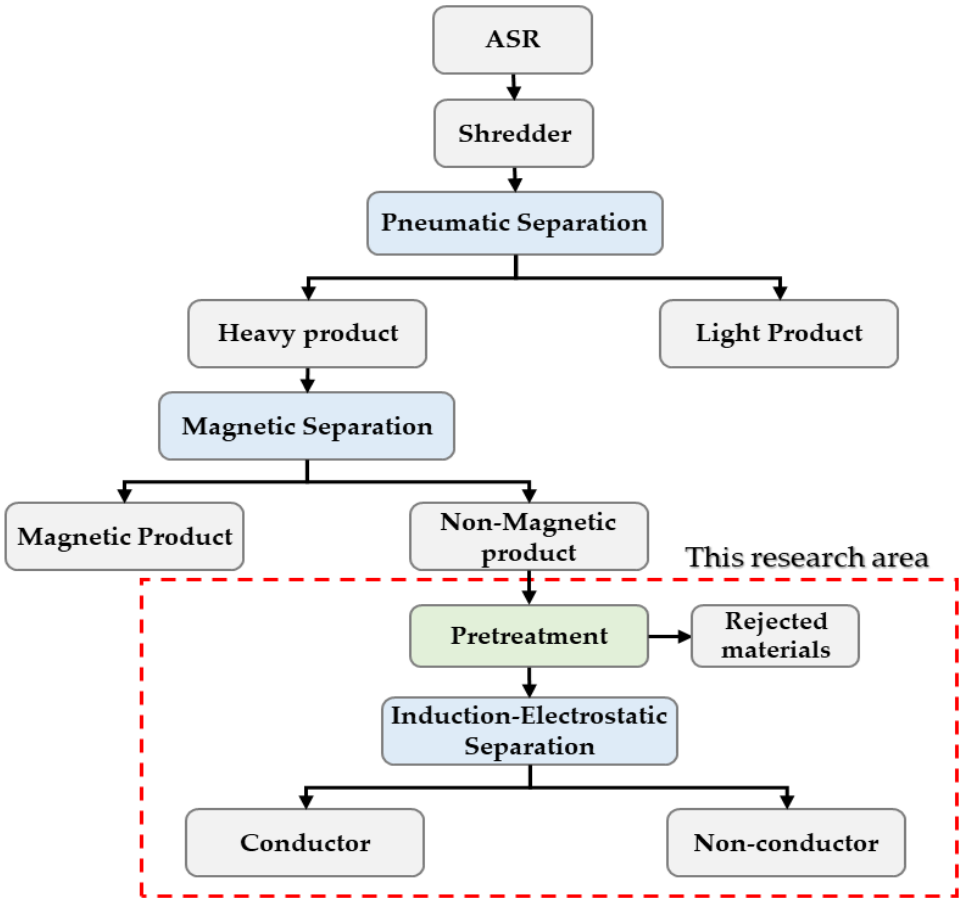

Figure 2. Flowchart of ASR separation process.

2.2.1. Pretreatment

The proposed pretreatment processes to remove any impurities attached to the glass particles can be described as follows:

→ Sieving was conducted using a 40 mesh screen for 5 min for the ASR sample. Then, any product that remained above the mesh after sieving was used for the separation test and any samples that fell through the mesh were discarded. The discarded materials were approximately 3% of all samples and consisted of numerous fine glass attaching the conductive material and other non-metals (plastics, etc.), and only a small amount of copper. The oversized materials consisted of glass and conductors, such as copper and aluminum.

→ Washing was carried out by stirring 50 g of the samples in a 2-L beaker filled with tap water at 2000 rpm for 10 min. Fluff, wood, and the fine powder attached to glass particles were floated on the surface during washing and their mass was less than 1% of all samples. The remaining materials were dried at 60 °C for 24 h.

→ Pyrolysis was performed by using an electric furnace (SF-30, Cerin Ceramics Co., Ltd, Namyangju, Korea). A crucible containing 50 g of the sample was placed in the furnace and heated for 2 h at a minimum temperature of 200 °C. After pyrolysis, the sample was allowed to cool by leaving it at room temperature (24 °C) for 24 h.

→ Oxidation was conducted by using a hydrogen peroxide solution (Duksan Pure Chemicals Co., Ltd., Ansan, Korea). The organic matter that had adhered to the glass particles was oxidized and removed by using hydrogen peroxide with a concentration of 0.5 M at 60 °C for 2 h, after which the sample was dried at 60 °C for 24 h.

→ Sieving/washing was performed as the combination of sieving and washing pretreatments described above.

2.2.2. Induction Electrostatic Separation

An induction-type electrostatic separator unit is shown in Figure 3 and consists of: (a) A feeder, (b) positive electrode, (c) negative electrode, (d) splitter and bins, and (e) feed rate controller. The positive electrode (induction plate) is a compound plate made of rubber and carbon, while the negative electrode is made of aluminum. The power supply (KSA-C) was a direct-current power source (max.: ±40 kV), and the relative humidity was controlled using a dehumidifier (SDH-LX200, Shinil Corp., Seoul, Korea). The initial charge of the particles was neutralized with a discharger (Kasuga Denki Inc., Kawasaki, Japan).

A pretreated ASR sample was fed to the positive electrode plate from the feeder and the conductors were positively charged with the positive electrode while they vibrated toward the edge of the electrode, whereas the net charge on the non-conductors remained unchanged. When the material reached the end of the positive electrode, the conductors were repelled by a positive electrode of the same polarity and deflected toward the negative electrode, due to the electric field between the electrodes. The non-conductors fell freely off the edge of the positive electrode. Finally, the conductors and non-conductors were separated by the splitter and collected into separate bins.

For checking the tribocharging effect before induction electrostatic separation, the charge density (nC/g) of copper, glass, and copper/glass (ratio of 10:90) samples, passed onto the surface electrode by vibration (without applied voltage), were measured by using a Faraday cage (KQ-1400, KASUGA DENKI, Inc., Kawasaki, Japan). The results were −4.075 nC/g, −0.24 nC/g, −0.85 nC/g for copper, glass, and copper/glass, respectively. The charge density of the two samples (glass and copper/glass) was negligible, except that of copper. In addition, the effect of induction charging was overwhelming because of the direct induction of high voltage coming from the electrodes, compared to the tribocharging between materials or the material and tribocharger. Therefore, turbocharging is considered to have no effect.

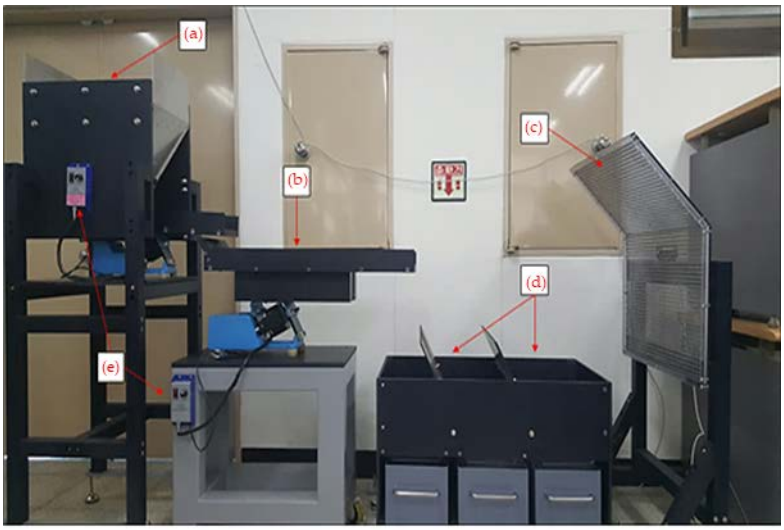

Figure 3. Photograph of the induction electrostatic separation unit: (**a**) Feeder, (**b**) positive electrode, (**c**) negative electrode, (**d**) splitter and bins, and (**e**) feed rate controller.

Each electrostatic separation test was duplicated and the separation performance was evaluated by handpicking. The values of the variables during the tests on the induction-electrostatic separator are listed in Table 2.

Table 2. Parameters used in the induction electrostatic separator.

Experimental Conditions	
Feed rate (g/min)	50
Distance between electrode (m)	0.6
Initial speed (m/s)	0.13
Applied voltage (kV)	10, 20, 30, 40
Relative humidity (%)	35, 45, 55, 65
Splitter position (cm)	7, 8, 9, 10

2.2.3. Particle Trajectory Analysis

A flowchart of the particle trajectory analysis method is shown in Figure 4. When the electrostatic separation conditions were supplied as input to the particle trajectory analysis, the electric field was calculated based on the input data and used to plot the movement of the particles on a Cartesian coordinate system. Then, the trajectories of the particles were determined by accumulating the positional changes of the particles. The theoretical background of the method and the details of the trajectory computation have been provided in a previous paper [23].

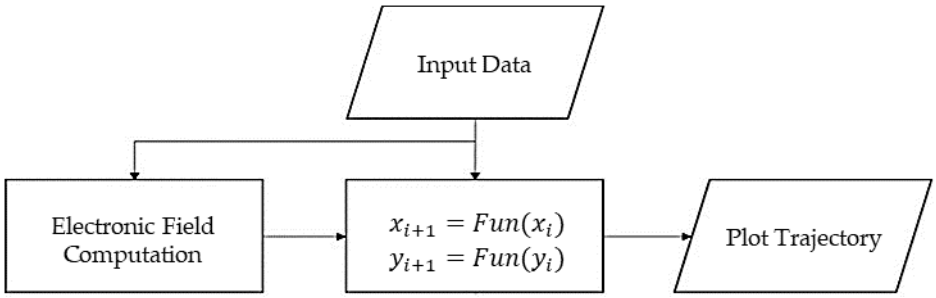

Figure 4. Flowchart of the particle trajectory analysis method.

In the particle trajectory analysis, the shapes of the copper wires and glass particles were simplified before modeling, since the weight and charge on the particles vary depending on their shape and size.

As shown in Figure 5, the shape of the glass particles was assumed to be a perfect sphere with a radius r, and the copper wire was assumed to be cylindrical with a radius r and length l.

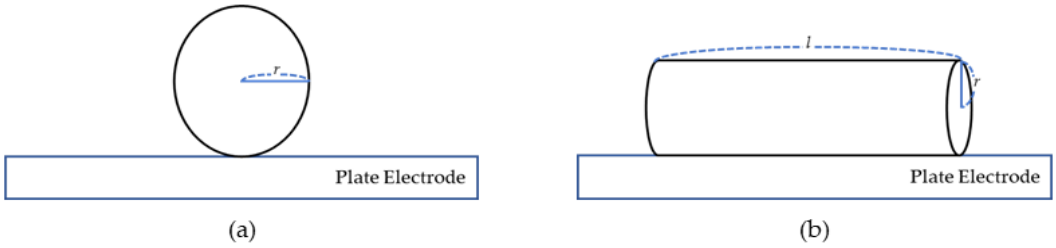

Figure 5. Simplified particle shapes: (**a**) A glass particle, and (**b**) a copper particle.

The forces acting on each particle in the induction electrostatic separator consist of electrostatic force F_e, gravitational force F_g, and air drag force F_d, and can be computed as follows:

$$F_e = QE, \tag{1}$$

$$F_g = mg, \tag{2}$$

$$F_d = 6\pi\eta rV. \tag{3}$$

where Q is the surface charge of the particle, E is the electric field strength, m is the mass of the particle, g is the acceleration due to gravity, η is the viscosity of air (1.85×10^{-5} Ns/m), r is the radius of the particle, and V is the velocity of the particle.

The three forces acting on a particle can be divided into horizontal and vertical components, and the total horizontal component is the sum of the electrostatic and air drag forces. Note that the direction of the electrostatic force is opposite to that of the air drag force. The total vertical force is the sum of the electrostatic, air drag, and gravitational forces in the vertical direction. Note that the electrostatic and air drag forces act upward in opposition to the gravitational force, which is the strongest force operating in the downward direction. The horizontal and vertical forces can be computed using Equations (5) and (6).

$$F = \sqrt{{F_x}^2 + {F_y}^2} = \sqrt{{ma_x}^2 + {ma_y}^2}, \tag{4}$$

$$F_x = F_e - F_d, \tag{5}$$

$$F_y = F_e + F_d - F_g. \tag{6}$$

In the analysis, the particle trajectories were mapped onto a Cartesian coordinate system and the forces acting on the particles in the system were translated into vectors in the x and y directions. The trajectories of each particle were then simulated by using the forces acting on each vector. The location of each particle was determined based on the acceleration and velocity at a specific instant of time relative to the immediately preceding particle position. The speed and acceleration of each particle were computed by using the sum of the corresponding directional forces. The directional acceleration of each particle can be computed by using Equations (9) and (10).

$$x_{i+1} = x_i + \mathrm{V_x}(x_i, y_i)dt + 0.5a_x(x_i, y_i)dt^2, \tag{7}$$

$$y_{i+1} = y_i + \mathrm{V_y}(x_i, y_i)dt + 0.5a_y(x_i, y_i)dt^2, \tag{8}$$

$$a_\mathrm{x}(x_i, y_i) = \frac{\mathrm{Q}E_x(x_{i-1}, y_{i-1}) - 6\pi\eta rV_x(x_{i-1}, y_{i-1})}{m}, \tag{9}$$

$$a_\mathrm{y}(x_i, y_i) = \frac{\mathrm{Q}E_y(x_{i-1}, y_{i-1}) + 6\pi\eta rV_y(x_{i-1}, y_{i-1})}{m} - g. \tag{10}$$

3. Results

3.1. Separation Test

A pretreatment process involving sieving, washing, pyrolysis, oxidation, and sieving/washing. as described in Section 2.2.1. was performed to remove the impurities that adhered to the glass in the raw sample. If left in place, these impurities would degrade the electrostatic separation efficiency. The results of electrostatically separating the pretreated ASR samples are shown in Figure 6. Here, the tests were conducted by using an applied voltage of 30 kV, 45% relative humidity, splitter position at 9 cm, and distance of 60 cm between the two electrodes. As shown in the figure, the efficiency of the electrostatic separation for the pretreated samples was better than that of the raw ASR samples. In fact, the grade of the pretreated samples was more than twice the grade of the raw samples, which had achieved a 25.6% grade. In addition, the efficiency of electrostatic separation by sieving/washing was the highest with a 76% grade and 85% recovery. Based on these results, the combination of sieving and washing was found to be more effective than sieving and washing as individual processes, because the combined process performed better in terms of removing the fine conductive particles that had adhered to the glass. The results of the pyrolysis and oxidation appeared inefficient in terms of the separation efficiency and economic cost. Thus, the remaining experiments in this study, which were conducted to optimize the induction electrostatic separation process, employed ASR pretreated by sieving/washing.

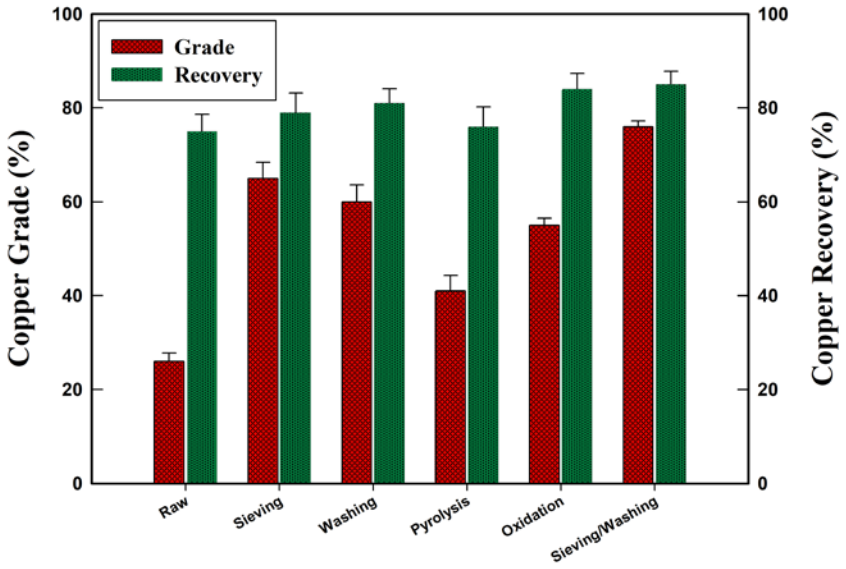

Figure 6. Comparison of electrostatic separation on ASR samples pretreated by sieving, washing, pyrolysis, oxidation and sieving/washing (an applied voltage of 30 kV, splitter position at 9 cm, relative humidity of 45%, and distance of 60 cm between the electrodes).

The results of the experiments based on ASR pretreated by sieving/washing and the corresponding parameters, such as the applied voltage, relative humidity, and splitter position, are depicted in Figures 7–9. The effects of the applied voltage on the grade and recovery of copper are shown in Figure 7. The test conditions can be summarized as follows: Applied voltage10–40 kV, relative humidity 35%, splitter position at 8 cm, and distance of 60 cm between the two electrodes. Based on the results, at 10 kV, the separation efficiency of copper was low with a 60% grade and 58% recovery, while at 20 kV, it was the highest at 83.1% grade and 91.4% recovery. In terms of the trend, the grade of copper decreased as the applied voltage increased from 30 to 40 kV. Upon inspection, it appeared that some glass remained attached to the conductive materials even after the ASR was pretreated. Ideally, if all of the conductive material attached to the glass was perfectly removed, then

the grade of copper would have increased as the applied voltage increased. However, it was actually observed that, above an applied voltage of 20 kV, the grade of copper actually decreased. This indicates that some glass particles, which behaved similar to the conductive particles, remained in the samples.

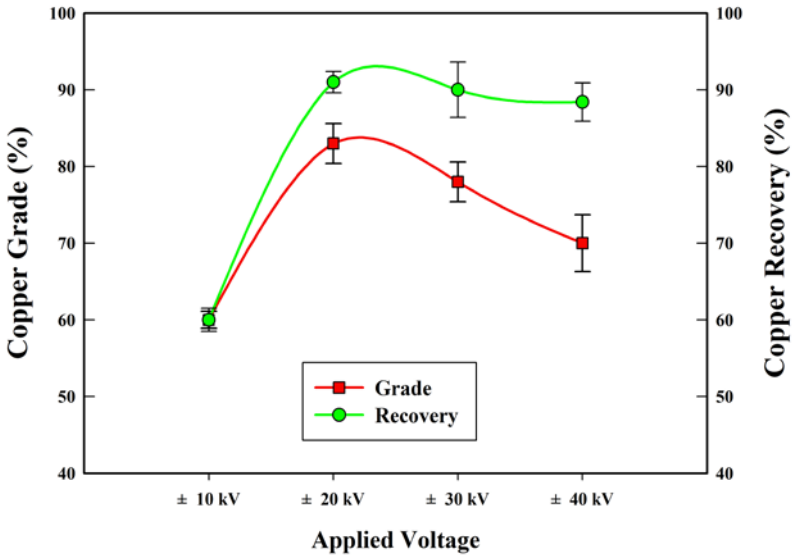

Figure 7. Effects of the applied voltage on the grade and recovery of copper after sieving/washing (splitter position: 8 cm, relative humidity: 35%, distance between electrodes: 60 cm).

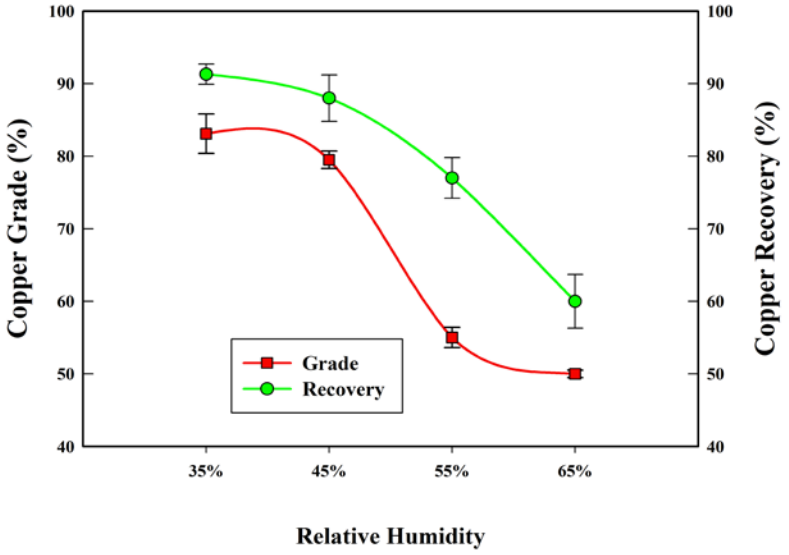

Figure 8. Effect of relative humidity on grade and recovery of copper in induction electrostatic separation after sieving/washing (applied voltage: 20 kV, splitter position: 8 cm, distance between electrodes: 60 cm).

The effect of the relative humidity on the grade and recovery of copper is shown in Figure 8. The test conditions were as follows: Relative humidity of 35–65%, applied voltage of 20 kV, splitter position at 8 cm, and distance of 60 cm between two electrodes. From the results, the separation efficiency of copper was found to be the highest when the relative humidity was below 35%. However, the efficiency decreased as the relative humidity increased, especially from 55 to 65%, which was probably caused by the charge density of copper decreasing as the relative humidity increased.

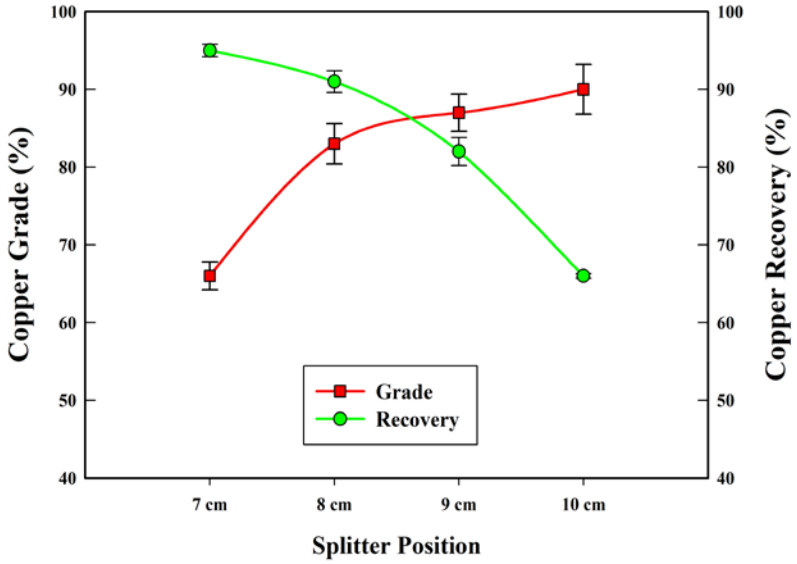

Figure 9. Effect of splitter position on grade and recovery of copper in induction electrostatic separation after sieving/washing (applied voltage: 20 kV, relative humidity: 35%, distance between electrodes: 60 cm).

Generally, relative humidity is considered to affect the conductivity of both air and particles [24–27]. Both voltage and current coming from electrodes reduce with increasing humidity, because these are consumed by the water droplets in the air, and thus the humidity may disturb the charging of the particles. Moreover, water attached to the surfaces of the materials may charge glass (non-conductor) and discharge copper rapidly, (conductor) whose conductivity is large. It is assumed that water (moisture) attached to the surfaces of the conductors (coppers) discharged their charge and then the copper particles that had a relatively low charge, due to the relative humidity were less deflected toward the vertical plate negative electrode. On the other hand, it appears that the conductivity of glass increased, due to the water on its surface, with increasing humidity and then some small glass particles tended to move toward the negative electrode, degrading the separation efficiency. In this test, it was possible to achieve an acceptable separation efficiency of copper as long as the relative humidity was less than 35%. Based on these results, it can be concluded that the relative humidity is an important factor in the separation of conductor and non-conductor particles.

The effect of the splitter position on the grade and recovery of copper is shown in Figure 9. The test conditions were as follows: The splitter position was 7–10 cm, relative humidity was 35%, the applied voltage was 20 kV, and the distance between the two electrodes was 60 cm. As shown in the figure, the copper grade increased and the recovery decreased as the splitter position moved from the positive electrode toward the negative one. A copper grade of 83.1% and recovery of 90.4% were obtained at a splitter position of 8 cm from the center to the negative electrode, which appeared to be the optimum position. However, a copper purity of approximately 90% was obtained at a splitter position of 10 cm from the center to the negative electrode, although the copper recovery at this point was reduced by 23.9%. The falling position of the particles was observed to vary depending on the electric field strength, charge density, particle size, shape, relative humidity, gravitational force, and drag force [17,22,23,28]. This is because copper particles that have a high charge density will be strongly deflected toward the negative electrode while copper particles that have a neutral or low charge density will either fall freely or be weakly deflected.

In the case of the glass particles, dielectric glass particles will be not deflected toward the negative electrode. However, glass particles that remain attached to conductive materials even after pretreatment may exhibit a behavior similar to that of copper and thereby degrade the separation efficiency.

3.2. Trajectory Analysis

The trajectories of the conductor (copper) and non–conductor (glass) particles after pretreatment were simulated and observed in comparison to the trajectories of raw samples (especially raw glass). These are plotted in Figure 10 for an applied voltage of 20 kV, relative humidity of 35%, distance of 60 cm between the two electrodes, and an initial speed of 0.13 m/s. As can be seen in the copper trajectories, the distance moved by the copper tended to increase toward the negative electrode as the particle size *r* decreased from 0.25 to 0.06 mm. The trajectories of the large particles (0.25 mm) were relatively similar in both the observations and simulation. However, the observed trajectories of the small particles (0.06 mm) moved closer to the negative electrode than in the simulation. In terms of the deviation trajectories of the small copper particles, the separation performance of copper improved as the particles moved further into the copper collection zone. Thus, the differences between the observations and simulation of the small particles were not considered significant. On the other hand, in the case of glass, the observed trajectories of the large particles (0.5 mm) were similar to those in the simulation and were not deflected toward the negative electrode. However, the observed trajectories of the small glass particles (0.16 mm) were seen to move toward the negative electrode. It appears that in the case of the small particles, the conductive material that affected the separation efficiency of copper was not perfectly removed by the pretreatment. To investigate this further, a trajectory analysis with the glass particle size before and after pretreatment was performed.

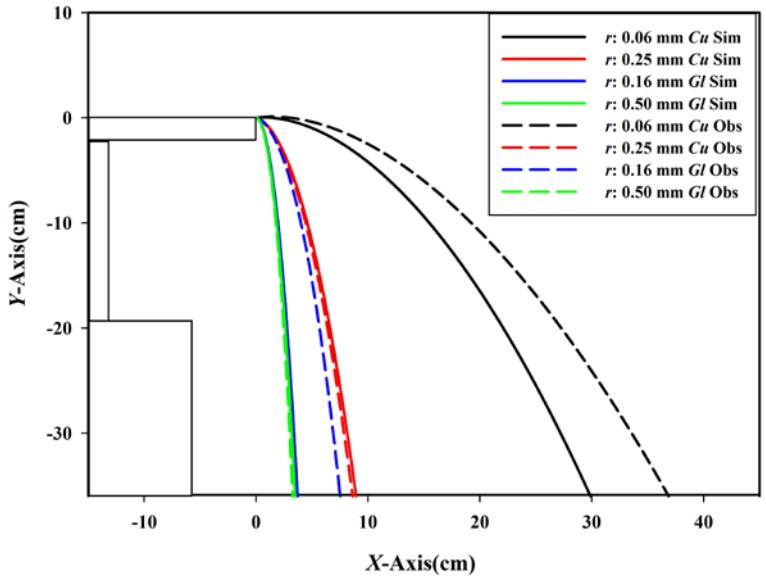

Figure 10. Observed (Obs) vs. simulated (Sim) trajectories of cylindrical copper (Cu) and spherical glass (*Gl*) pretreated by sieving/washing (applied voltage: 20 kV, relative humidity: 35%, distance between electrodes: 60 cm, initial speed: 0.13 m/s).

The observed trajectories of the raw versus pretreated glass particles are plotted in Figure 11 for the following conditions: An applied voltage of 20 kV, relative humidity of 35%, distance of 60 cm between two electrodes, and initial speed of 0.13 m/s. The results plotted in Figure 11 show that the movement distance of the pretreated glass particles toward the negative electrode was considerably smaller than that of the raw glass, which indicates that the copper grade was improved by pretreatment. The trajectories of the pretreated large particles (0.5 and 0.36 mm) were observed to be similar to the free-fall curve while the pretreated small particles (0.16 mm) still moved toward the negative electrode, which affected the separation efficiency of the copper despite the reduction in the deflection difference for these particles compared to raw glass. This suggests that for large particles, most of the conductive material was removed by pretreatment, while for the small particles, enough remained to influence the separation efficiency.

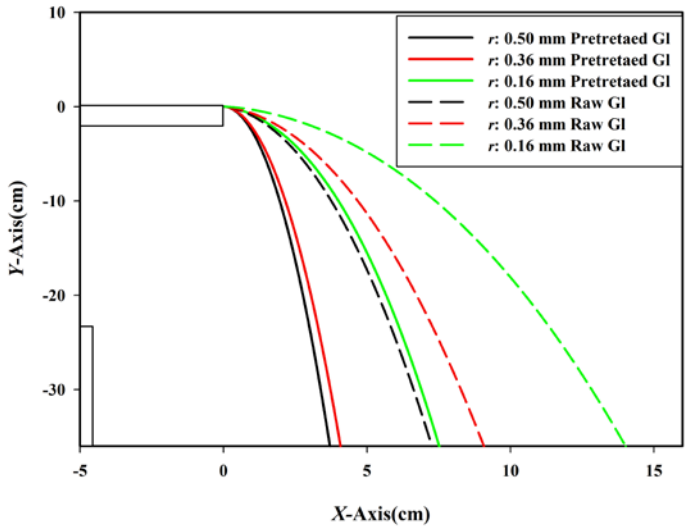

Figure 11. Observed trajectories of raw vs. pretreated glass (applied voltage: 20 kV, relative humidity: 35%, distance between electrodes: 60 cm, initial speed: 0.13 m/s).

The observed and simulated trajectories of the pretreated large and small glass particles are plotted in Figure 12, where it can be seen that the average observed trajectory of 0.5 mm glass particles was similar to the simulated trajectory. However, the observed average trajectory of the 0.16 mm glass particles at a splitter position of 8 cm, which was considered according to Figure 9, was significantly different from the simulated average trajectory. To investigate this further, the individual observed trajectories for the pretreated various glass particles with sizes between 0.16 and 0.5 mm are shown in Figure 13. In the case of the large particles, the ones that did not exceed a fiducial position of 8 cm did not move into the copper collection zone. On the other hand, some of the small particles moved beyond a fiducial position of 8 cm. There is a strong possibility that the small glass particles increased in size when additional conductive materials became mechanically attached to the surface of the glass in the shredding process, which led to a greater influence of the electrostatic force on them than gravitational force when compared to large particles. Upon further analysis, it was confirmed that small glass particles, approximately 10% by mass, were contained in the extracted copper product.

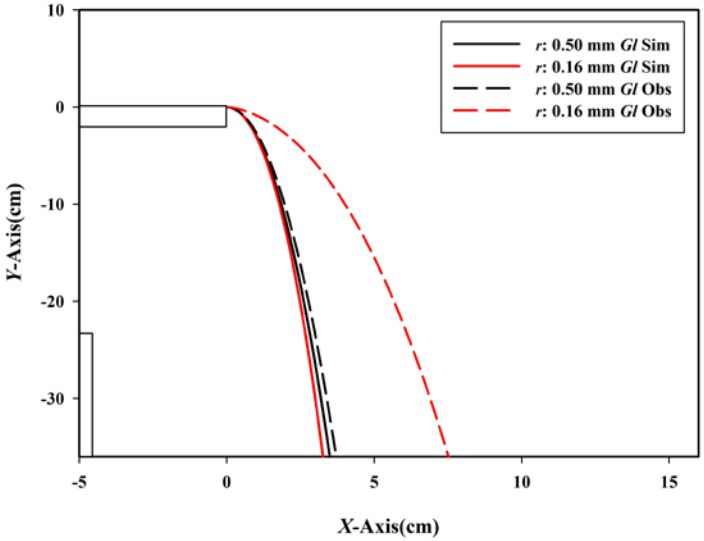

Figure 12. Observed vs. simulated trajectories of pretreated large and small glass (*Gl*) particles (applied voltage: 20 kV, relative humidity: 35%, distance between electrodes: 60 cm, initial speed: 0.13 m/s).

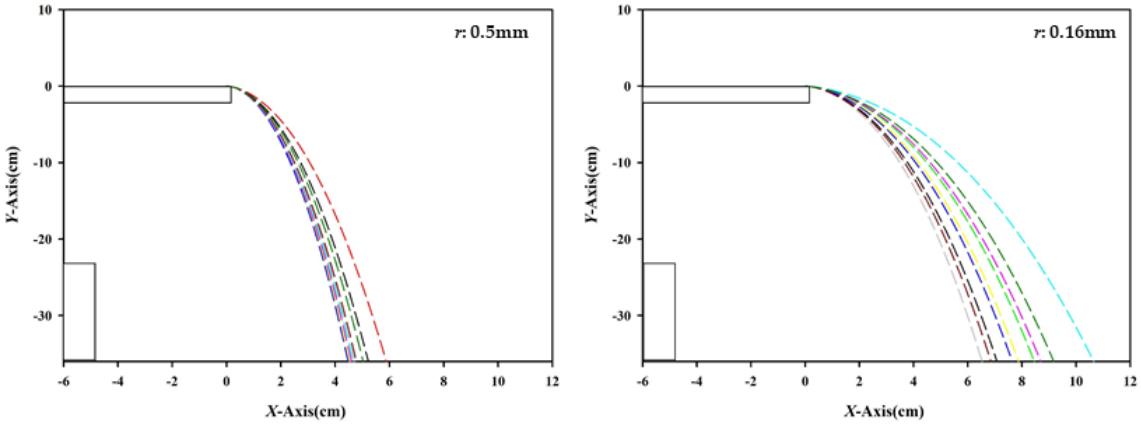

Figure 13. Observed trajectories of various large and small pretreated glass particles (applied voltage: 20 kV, relative humidity: 35%, distance between electrodes: 60 cm, initial speed: 0.13 m/s).

The results of the induction electrostatic separation for raw and pretreated ASR are compared in Figure 14 for the following test conditions: An applied voltage of 20 kV, relative humidity of 35%, splitter position of 8 cm, and distance of 60 cm between two electrodes. As shown in the figure, the efficiency of the electrostatic separation for pretreated ASR was superior to that of raw ASR. For the raw ASR, the separation efficiency of copper was very poor, with a 34.3% grade and 58.6% recovery, while for the pretreated ASR, the grade increased to 83.1% and the recovery to 90.4%, although the separation efficiency was slightly reduced when some of the small glass particles became attached to the conductive materials. Based on these results, it is evident that the sieving/washing pretreatment process improved the efficiency of electrostatic separation for ASR and effectively removed any conductive materials that adhered to the glass during shredding.

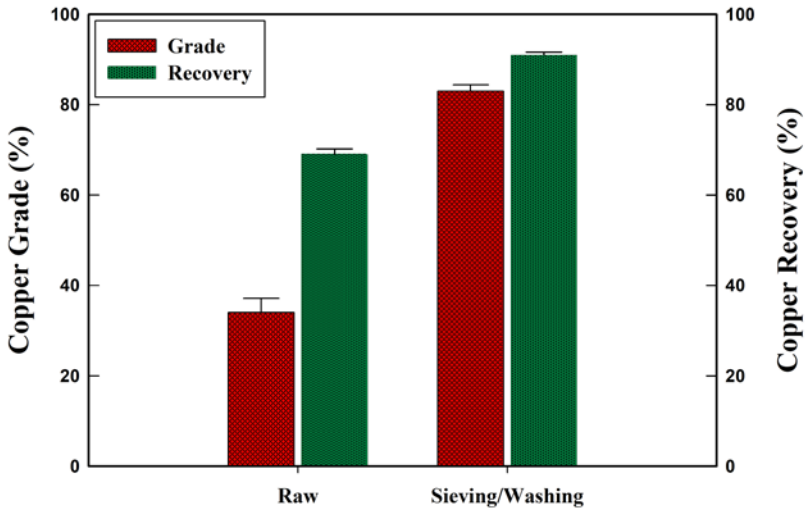

Figure 14. Comparison of induction electrostatic separation on raw vs. pretreated (sieving/washing) ASR (applied voltage: 20 kV, splitter position: 8 cm, relative humidity: 35%, distance between electrodes: 60 cm).

4. Conclusions

The proposed pretreatment processes, which involved sieving, washing, pyrolysis, oxidation, and sieving/washing, were evaluated by electrostatic separation efficiency, and of all the process, the sieving/washing was found to be most effective for removing extraneous conductive materials. When tested, the optimum separation efficiency of copper was achieved at an applied voltage of 20 kV, relative humidity below 35%, and an 8 cm splitter position. The pretreatment effect and separation

efficiency were evaluated by analyzing the trajectories of the copper and glass particles. The trajectories of the copper particles were found to be quite similar in both the observation and simulation; however, some of the small glass particles were found to have moved beyond a fiducial position of 8 cm, which deteriorated the separation efficiency of copper. A subsequent content analysis of the conductive materials confirmed that the copper product contained small glass particles amounting to 10% by mass. The efficiency of the electrostatic separation for pretreated ASR was superior to that of raw ASR. Specifically, the separation efficiency of copper for pretreated ASR increased significantly to a grade of 83.1% and a recovery of 90.4% compared to that of raw ASR (34.3% grade and 58.6% recovery), although the separation efficiency was slightly reduced by the small glass particles that remained attached to the conductive materials. This demonstrates that the sieving/washing process effectively removed the conductive materials that had adhered to the glass during the shredding process. In conclusion, the proposed pretreatment and electrostatic separation technique was found to improve the separation efficiency of ASR. An area of future research is to develop a more advanced particle trajectory simulation that includes computation of the electric field and considers the other forces acting on the particles.

Author Contributions: C.-H.P., B.-U.K. conceived and designed the experiments; B.-U.K. performed the experiments; C.-H.P., B.-U.K. analyzed the data; C.-H.P. wrote the paper.

Funding: This research received no external funding.

Conflicts of Interest: The authors declare no conflict of interest.

Nomenclature

E	Electric field strength (V/m)
F_d	Air drag force (N)
F_e	Electric force (N)
F_g	Gravity force (N)
g	Acceleration due to gravitation (m/s^2)
l	Length of the particle (m)
m	Mass of the particle (kg)
Q	Quantity of electricity (C)
r	Radius of the particle (m)
V	Velocity of particle (m/s)
η	Viscosity of Air (Ns/m^2)

References

1. Cossu, R.; Lai, T. Automotive shredder residue (ASR) management: An overview. *Waste Manag.* **2015**, *45*, 143–151. [CrossRef] [PubMed]
2. Korea, M.O.E.O. Act on resource circulation of electrical and electronic equipment and vehicles. Available online: ttp://www.law.go.kr/lsInfoP.do?lsiSeq=188594&urlMode=engLsInfoR&viewCls=engLsInfoR#0000. (accessed on 25 October 2018).
3. Parliament, E. Directive 2000/53/EC of the european parliament and of the council of 18 September 2000 on end-of life vehicles. *Off. J. Eur. Communities* **2000**, *21*, L269.
4. Sakai, S.-I.; Noma, Y.; Kida, A. End-of-life vehicle recycling and automobile shredder residue management in japan. *J. Mater. Cycles Waste Manag.* **2007**, *9*, 151–158. [CrossRef]
5. Kim, K.-H.; Joung, H.-T.; Nam, H.; Seo, Y.-C.; Hong, J.H.; Yoo, T.-W.; Lim, B.-S.; Park, J.-H. Management status of end-of-life vehicles and characteristics of automobile shredder residues in korea. *Waste Manag.* **2004**, *24*, 533–540. [CrossRef] [PubMed]
6. Santini, A.; Passarini, F.; Vassura, I.; Serrano, D.; Dufour, J.; Morselli, L. Auto shredder residue recycling: Mechanical separation and pyrolysis. *Waste Manag.* **2012**, *32*, 852–858. [CrossRef] [PubMed]
7. Kuwayama, Y.; Ito, M.; Hiroyoshi, N.; Tsunekawa, M. Jig separation of crushed automobile shredded residue and its evaluation by float and sink analysis. *J. Mater. Cycles Waste Manag.* **2011**, *13*, 240–246. [CrossRef]

8. Alunno Rossetti, V.; Di Palma, L.; Ferraro, A. Production and characterization of aggregate from nonmetallic automotive shredder residues. *J. Mater. Civ. Eng.* **2010**, *23*, 747–751. [CrossRef]
9. Fabrizi, L.; Bevilacqua, P. Wire separation from automotive shredder residue. *Phys. Sep. Sci. Eng.* **2003**, *12*, 145–165. [CrossRef]
10. Lee, H.-Y.; Oh, J.-K. A study on the shredding of end-of-life vehicles and materials separation. *Geochem. Eng.* **2003**, *6*, 100–105. [CrossRef]
11. Tripathy, S.K.; Ramamurthy, Y.; Kumar, C.R. Modeling of high-tension roll separator for separation of titanium bearing minerals. *Powder Technol.* **2010**, *201*, 181–186. [CrossRef]
12. Tilmatine, A.; Medles, K.; Bendimerad, S.-E.; Boukholda, F.; Dascalescu, L. Electrostatic separators of particles: Application to plastic/metal, metal/metal and plastic/plastic mixtures. *Waste Manag.* **2009**, *29*, 228–232. [CrossRef] [PubMed]
13. Wu, J.; Li, J.; Xu, Z. Electrostatic separation for recovering metals and nonmetals from waste printed circuit board: Problems and improvements. *Environ. Sci. Technol.* **2008**, *42*, 5272–5276. [CrossRef] [PubMed]
14. Vlad, S.; Mihailescu, M.; Rafiroiu, D.; Iuga, A.; Dascalescu, L. Numerical analysis of the electric field in plate-type electrostatic separators. *J. Electrostat.* **2000**, *48*, 217–229. [CrossRef]
15. Tilmatine, A.; Medles, K.; Younes, M.; Bendaoud, A.; Dascalescu, L. Roll-type versus free-fall electrostatic separation of tribocharged plastic particles. *IEEE Trans. Ind. Appl.* **2010**, *46*, 1564–1569. [CrossRef]
16. Richard, G.; Salama, A.R.; Medles, K.; Lubat, C.; Touhami, S.; Dascalescu, L. Electrostatic separation of two types of copper wires from electric cable wastes. In Proceedings of the 2016 Electrostatics Joint Conference, West Lafayette, IN, USA, 13–16 June 2016.
17. Mihailescu, M.; Samuila, A.; Urs, A.; Morar, R.; Iuga, A.; Dascalescu, L. Computer-assisted experimental design for the optimization of electrostatic separation processes. *IEEE Trans. Ind. Appl.* **2002**, *38*, 1174–1181. [CrossRef]
18. Labair, H.; Touhami, S.; Tilmatine, A.; Hadjeri, S.; Medles, K.; Dascalescu, L. Study of charged particles trajectories in free-fall electrostatic separators. *J. Electrostat.* **2017**, *88*, 10–14. [CrossRef]
19. Li, J.; Lu, H.; Xu, Z.; Zhou, Y. A model for computing the trajectories of the conducting particles from waste printed circuit boards in corona electrostatic separators. *J. Hazard. Mater.* **2008**, *151*, 52–57. [CrossRef] [PubMed]
20. Li, J.; Xu, Z.; Zhou, Y. Theoretic model and computer simulation of separating mixture metal particles from waste printed circuit board by electrostatic separator. *J. Hazard. Mater.* **2008**, *153*, 1308–1313. [CrossRef] [PubMed]
21. Lu, H.; Li, J.; Guo, J.; Xu, Z. Movement behavior in electrostatic separation: Recycling of metal materials from waste printed circuit board. *J. Mater. Process. Technol.* **2008**, *197*, 101–108. [CrossRef]
22. Wu, J.; Li, J.; Xu, Z. An improved model for computing the trajectories of conductive particles in roll-type electrostatic separator for recycling metals from WEEE. *J. Hazard. Mater.* **2009**, *167*, 489–493. [CrossRef] [PubMed]
23. Kim, B.-U.; Han, O.-H.; Jeon, H.-S.; Baek, S.-H.; Park, C.-H. Trajectory analysis of copper and glass particles in electrostatic separation for the recycling of ASR. *Metals* **2017**, *7*, 434. [CrossRef]
24. Kelly, E.; Spottiswood, D. The theory of electrostatic separations: A review part I. Fundamentals. *Miner. Eng.* **1989**, *2*, 33–46. [CrossRef]
25. Kelly, E.; Spottiwood, D. The theory of electrostatic separations: A review part II. Particle charging. *Miner. Eng.* **1989**, *2*, 193–205. [CrossRef]
26. Kelly, E.; Spottiswood, D. The theory of electrostatic separations: A review part III. The separation of particles. *Miner. Eng.* **1989**, *2*, 337–349. [CrossRef]
27. Dodbiba, G.; Shibayama, A.; Miyazaki, T.; Fujita, T. Electrostatic separation of the shredded plastic mixtures using a tribo-cyclone. *Phys. Sep. Sci. Eng.* **2002**, *11*, 63–92. [CrossRef]
28. Vlad, S.; Iuga, A.; Dascalescu, L. Numerical computation of conducting particle trajectories in plate-type electrostatic separators. *IEEE Trans. Ind. Appl.* **2003**, *39*, 66–71. [CrossRef]